Pergamon

Cement and Concrete Research 29 (1999) 1131–1147

CEMENT AND CONCRETE RESEARCH

The nature of C-S-H in hardened cements

I.G. Richardson*

Civil Engineering Materials Unit, School of Civil Engineering, University of Leeds, Leeds LS2 9JT, UK

Received 19 July 1999; accepted 23 July 1999

Abstract

Calcium silicate hydrates (C-S-H) are the main binding phases in all Portland cement-based systems. This paper considers the morphology, composition, and nanostructure of C-S-H in a range of hardened cements. Inner product (Ip) C-S-H present in larger Portland cement grains typically has a fine-scale and homogeneous morphology with pores somewhat under 10 nm in diameter. Ip from larger slag grains also displays this morphology, but is chemically distinct in having high content of Mg and Al. The hydrated remains of small particles—whether of Portland cement, slag or fly ash—contain a less dense product with substantial porosity surrounded by a zone of relatively dense C-S-H; this has implications for the analysis of porosity and pore-size distributions on backscattered electron images. In cement-slag blends, the fibrillar morphology of outer product (Op) C-S-H is gradually replaced by a foil-like morphology as the slag loading is increased. It seems likely that this change in morphology is largely responsible for the improved durability performance possible with slag-containing systems. The Ca/Si ratio of C-S-H in neat Portland cement pastes varies from ~1.2 to ~2.3 with a mean of ~1.75. The Ca/(Si + Al) ratio of C-S-H in water activated cement-slag pastes (0–100% slag) varies from ~0.7 to ~2.4; these limits are consistent with dreierkette-based models for the structure of C-S-H. Al substitutes for Si in C-S-H only in the "bridging" tetrahedra of dreierkette chains; this is true for a range of systems, including blends of Portland cement with slag, fly ash, and metakaolin. These data support Richardson and Groves' general model for substituted C-S-H phases. The bonding of C-S-H to other products of hydration is generally good.

Keywords: B. Calcium-Silicate-Hydrate (C-S-H); B. TEM; B. Microstructure; B. Backscattered electron imaging; NMR

1. Introduction

Calcium silicate hydrates (C-S-H) are the main binding phases in all Portland cement-based systems; their exact nature is central to the science of cement and concrete. This article presents data principally for the C-S-H phases present in neat Portland cements, in blends of Portland cement with ground granulated blast-furnace slag, and in alkali-hydroxide activated slags; data are also reported which illustrate the similarity of the C-S-H phases present in blends of Portland cement with fly ash and metakaolin to those with slag.

2. Experimental

2.1. Materials

Details of the materials used in this work are given elsewhere: ordinary Portland cement-granulated blast-furnace slag blends [1,2]; white cement-slag blends [3]; white cement-fly ash and white cement-metakaolin blends [4]; slags activated by KOH solution [5]; synthetic slag-glass [6]. White cement was needed for the nuclear magnetic resonance (NMR) spectroscopy work because of its low Fe content; the presence of paramagnetic ions causes peak broadening in NMR.

2.2. Specimen preparation and experimental details

The slag- and pozzolan-Portland cement blends were prepared by mixing the required amounts of solids with deionized water (water/solids (W/S) ratios given in the text or figure captions); the slurries were then placed in plastic tubes which were sealed in plastic bags before placing in cure baths set at 20°C (ordinary Portland cement-slag blends) or 25°C (blends of white cement with slag, fly ash, or metakaolin). The blends which were activated with KOH solution were also cured at 25°C [solution/solids (S/S) ratios given in the text or figure captions]. The neat slags which were activated with KOH solution were mixed at a S/S of 0.4 and cured at 20°C in a fog room. Details of sample preparation and experimental procedures for analytical transmission electron microscopy (TEM) and for X-ray mapping in an electron microprobe analyser (EMPA) are given else-

* Corresponding author. Tel.: +44-113-233-2331; fax: +44-113-233-2265.

E-mail address: i.g.richardson@leeds.ac.uk (I.G. Richardson)

0008-8846/99/$ – see front matter
PII: S0008-8846(99)00168-4

where [1,7]. Freshly ground samples were used for NMR. Specimens were ground to a powder and packed into zirconia rotors. Single-pulse ^{29}Si and ^{1}H-^{29}Si cross polarization (CP) spectra were acquired using Bruker MSL-200 (magnetic field 4.7 T; operating frequency of 39.76 MHz for ^{29}Si) and MSL-300 (magnetic field 7.1 T; operating frequency of 59.62 MHz for ^{29}Si) spectrometers. The single pulse spectra were acquired over 2000→32000 scans using flip angles (30→45°) and pulse recycle delays (2→20s) sufficient to minimize saturation of the hydrate peaks. For CP, the Hartmann-Hahn condition was set using kaolinite [8]. ^{29}Si chemical shifts are given relative to tetramethylsilane at 0 ppm, with kaolinite used as an external standard at −91.2 ppm. All spectra were apodized with 10 Hz of exponential line broadening and zero filled to 8192 points prior to Fourier transformation. The spectra were iteratively fitted to voigt line shapes using the software Igor with additional macros written by Brough [9]. The full procedure is outlined in [3]. The experimental details for the trimethylsilylation (TMS) work are given in Lu et al. [10].

3. Results and discussion

3.1. Morphology and spatial distribution of C-S-H

3.1.1. Reference microstructure

Forty years ago Taplin [11] thought it "convenient to designate those products which lie within the original boundaries of the clinker particles 'inner' products, and those which lie 'outside' 'outer' products." The scheme has been adopted widely (a few examples are [2,7,12–19]) and, although there is not necessarily an exact correspondence between the positions of the outer boundaries of inner product (Ip) and the original grains [20], it is straightforward and is well-supported for a range of cement systems by evidence from the high resolution technique of transmission electron microscopy (TEM) [1,2,3,7,20–28] and by X-ray mapping of flat polished sections (using Mg as a chemical marker) [1,2,29,30]. More recently, Diamond and Bonen [31]—who considered "inner" and "outer products" to be poorly suited as descriptive terms—proposed a new nomenclature based on the interpretation of backscattered electron images of flat polished sections. They suggested two primary morphological entities; "phenograins" and "groundmass," with the most important distinction being the gross porosity of the groundmass and the size of the phenograins. Phenograins were defined as any distinct grain greater than around 10μm in size embedded in the groundmass. They could be composed of several different classes of material: "superficially, partially, or fully hydrated clinker grains, distinguishable crystals of calcium hydroxide, or filler particles in some cements." The groundmass was defined as " . . . CSH in either skeletal or amorphic form embedded in intersecting pores." The solid part of the groundmass would be composed of " . . . CSH, CH, and smaller amounts of calcium monosulfoaluminate hydrates, ettringite, and other phases;" these phases are generally not well-resolved by backscattered electron imaging. Much valuable information has been gained using this technique, but the utility of a classification system based solely on the interpretation of images with such modest resolution is limited. This is well-illustrated, for example, by Taylor's observation [32,33]—cited by Diamond and Bonen in support of their classification—that fully hydrated small grains become indistinguishable from outer product (Op); in fact, most are readily observed in the TEM [1,2,25]. The direct imaging of thinned sections in the TEM, which is a much higher resolution technique, has provided a good understanding of the composition and spatial distribution of the phases present in hardened cements, including the levels at which different phases are intermixed. Given this knowledge, the phenograin-groundmass classification would seem to have little application outside the description of backscattered electron images. As a drawback, it introduces yet another set of terminology to Cement Science.

3.1.2. Morphology of Ip C-S-H formed within larger grains (>∼5 μm)

TEM has shown that the Ip C-S-H present in larger cement grains typically has a fine-scale and homogeneous morphology. An example of Ip C-S-H with this morphology is shown in Fig. 1; this Ip region also contains some unreacted belite and CH. The scale of the fine porosity in this Ip is very difficult to determine since at higher magnification the pores coarsen rapidly in the electron beam [2,20]; the high Ca/Si ratio C-S-H present in hardened Portland cement pastes is particularly unstable. It is possible to take an image at low magnification (say, ×20 000) and then enlarge a region. Groves published such a micrograph from a hardened C_3S paste (Fig. 4 of [20]); he considered that the areas of light contrast—which had diameters somewhat under 10 nm—might be interpreted simplistically as voids. While the C-S-H had been dried aggressively during specimen preparation, this size of pore corresponded reasonably well to the results from small-angle neutron scattering experiments [34,35]. An example similar to Groves' Fig. 4, but from an alite grain in a Portland cement paste, is shown in Fig. 2. An example of Ip C-S-H which had coarsened in the electron beam, in this case in a hardened Portland cement paste, is shown in Fig. 3 [36]. Great care should be exercised when manipulating ion-thinned cement specimens in the TEM because it is quite possible for an operator to be unaware that damage has occurred [2]. It is of interest, in this respect, to note the similarity of the Ip C-S-H in Fig. 3 to that in Fig. 1(a) of Viehland et al. [28]. The Ip in Viehland et al.'s figure also appears to have experienced much beam damage. It is possible that the nanocrystalline regions reported later in their paper actually represent a decomposition product rather than C-S-H. In support of this view, it is notable that in a later study Viehland et al. [37] were unable to obtain comparable images for the crystalline calcium silicate hydrates 1.4 nm tobermorite and jennite which would be expected to be much more stable in the electron beam than

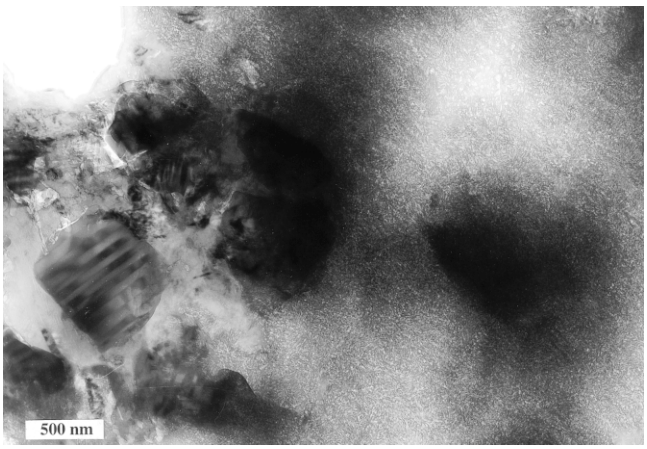

Fig. 1. Transmission electron micrograph showing an Ip region in a mature Portland cement paste which contains Ip C-S-H with the fine-scale morphology (centre-right), unreacted belite (left), and CH (surrounding the belite).

high Ca/Si ratio Ip C-S-H. Indeed, Ewart et al. [38] found that tobermorite could be studied at moderate magnifications (say, ×50 000) for quite long periods without evident loss of crystallinity or other damage; this is not possible with Ip C-S-H in hardened Portland cements [2]. When Ewart et al. attempted high resolution imaging of their tobermorite they observed lattice fringes, but only as a transient phenomenon. After the initial loss of lattice fringes from the hydrate crystal as it damaged, a more stable high resolution image developed which represented a decomposition product of the initial hydrate.

In Portland cement-slag blends—whatever the slag loading—or in alkali-hydroxide activated slags, Ip from larger slag grains commonly displays the typical compact fine-scale homogeneous morphology, but it is chemically distinct in having high content of Mg and Al [1,3,25–27]; laths or platelets are also often observed which are particularly rich in Mg and Al [1,25,26,39–41]. Slag Ip with the fine-scale homogeneous morphology and Op C-S-H with the fine foil-like morphology as observed in the TEM and scanning electron microscope (SEM) are shown in Fig. 4 (slag activated with 5*M* KOH hydrated for 12 months at 20°C, S/S=0.4).

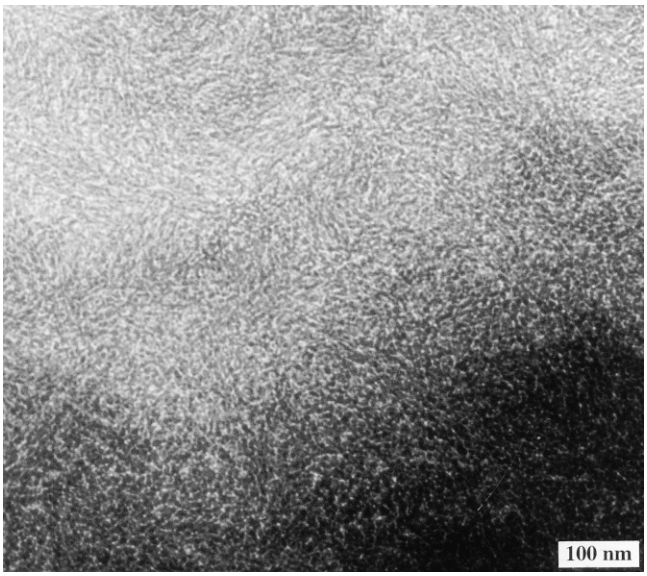

Fig. 2. Transmission electron micrograph showing Ip C-S-H in a Portland cement paste.

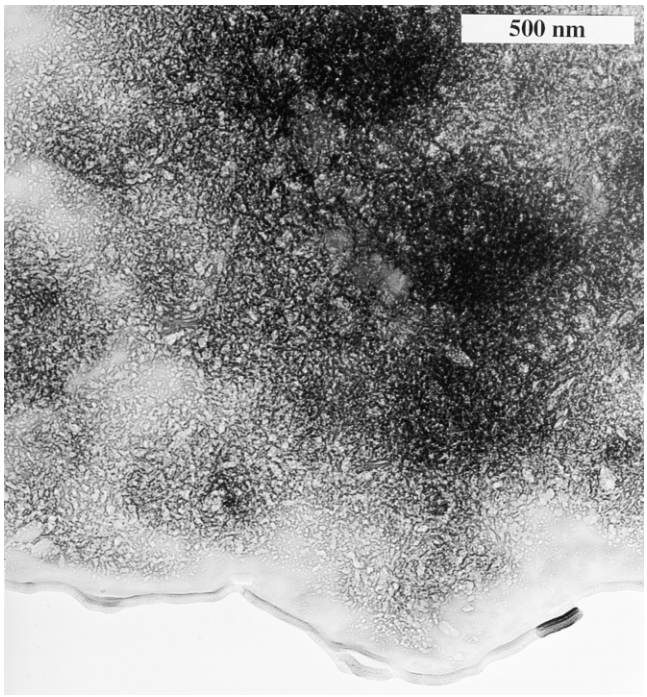

Fig. 3. Transmission electron micrograph showing Ip C-S-H in a mature Portland cement paste which had coarsened in the electron beam.

3.1.3. Morphology of Ip C-S-H in small fully hydrated grains (<∼5 μm)

The hydrated remains of relatively small particles—whether of Portland cement, slag, or fly ash—contain a less

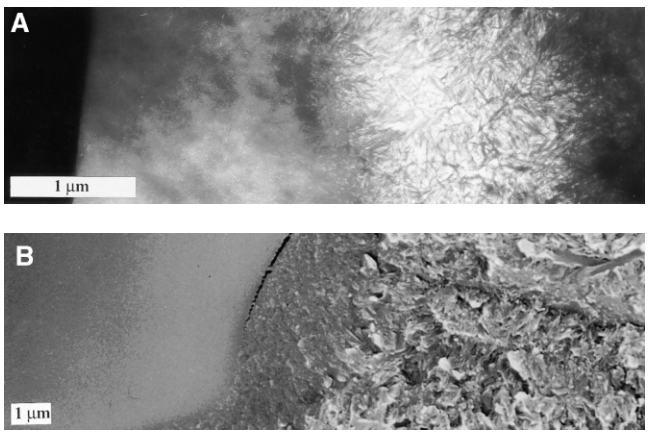

Fig. 4. TEM (a) and SEM (b) micrographs showing from left to right unreacted slag, Ip with the fine-scale compact morphology, and fine foil-like Op C-S-H in a mature KOH-activated slag paste.

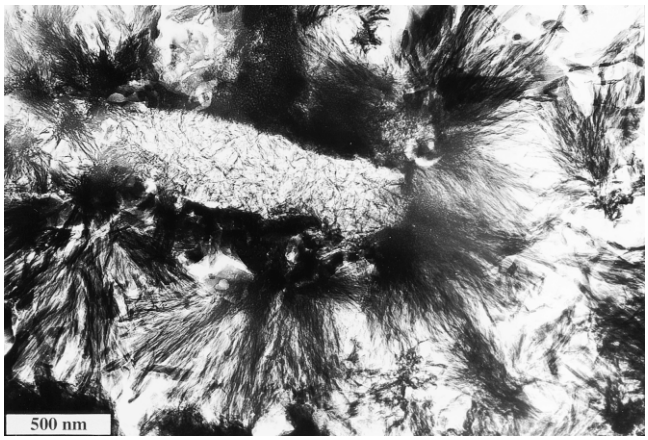

Fig. 5. Transmission electron micrograph showing low density Ip surrounded by a rim of relatively dense C-S-H and fibrillar Op C-S-H in a mature Portland cement paste.

dense product with substantial porosity, surrounded by a zone of relatively dense C-S-H [1,2,24,25]. Examples from TEM for alite, slag, and fly ash particles have been published previously [1,2,24,25]; an example for a Portland cement grain is shown in Fig. 5. For backscattered electron imaging cement samples must be sectioned, dried, impregnated with resin, and polished flat [42]. The relatively dense outer rim of these small particles may make it difficult for resin to penetrate the porous interior, which may then be removed during subsequent polishing. This is most likely for the smallest particles since they tend to have the most complete dense outer rims. Such grains would appear as isolated pores on the polished sections used for backscattered electron imaging. It is possible that many of the particles into which resin has penetrated may also be identified as isolated pores, or "hollow-shells," since the lower density C-S-H will appear dark on backscattered electron images. This is illustrated in Fig. 6(a), which shows a region of a Portland cement mortar. Careful examination of this image shows that most of the hollow shells contain some material. Fig. 6(b) is an enlargement of a part of the image which contains a small fully hydrated grain (centre-left) and the edge of a large partially hydrated grain (right). The small particle has a well-defined rim and there is material within its interior. The Ip is darker, and so less dense, than that present in the larger grain. In the analysis of backscattered electron images, the darkest shades of grey are taken to be porosity. In Figs. 6(c) and (d), the porosity was assigned arbitrarily as the lowest 32 bins of the greyscale histogram to show the most distinct pores; the corresponding pixels are represented as white on the images. Additional bins were assigned as porosity in Figs. 6(e) and (f). The threshold was chosen by comparison with the histograms and analysis techniques used by other workers [42,43,44] such that they would probably have assigned a similar number or fewer bins of the greyscale to porosity. Many of the white pixels fall within inner product regions: the interior of the fully hydrated particle in the enlarged area has been analysed as an $\sim 6 \times 4$ μm pore or "hollow shell." Since it is very likely that this grain contained a low density C-S-H with foil-like morphology, it is clear that porosity and pore-size information derived from the analysis of backscattered electron images should be interpreted with care.

3.1.4. Morphology of Op C-S-H

Jennings et al. [22] introduced a classification of C-S-H morphology based on observations in the TEM of ion-thinned sections of hardened C_3S pastes, and compared it with an earlier one based on the secondary electron imaging of fracture surfaces [13]. Groves et al. [7], also using TEM, found it difficult to make a sharp distinction between Jennings et al.'s type 1 and type 3 morphologies, and preferred instead to characterize all Op C-S-H in hardened C_3S or portland cement as "fibrillar." Since the morphology of the C-S-H is affected by the amount of available space, it seems unlikely that there are just two distinct Op morphologies—such as Jennings et al.'s types 1 and 3—but rather fibrils possessing a range of aspect ratios dependent upon space constraints. Examples of fine fibrillar C-S-H are shown in Figs. 5 and 7 (top).

There has been some discussion in the literature, noted by Groves [45], as to whether the morphology of this Op C-S-H should be referred to as "fibrillar" or "crumpled-foil." "Fibrillar" is preferred by this writer, with "foil-like" reserved for the distinctive morphology of the low Ca/Si ratio Op C-S-H present in slag and pozzolan-containing systems, which lack the linear directional aspect characteristic of the high Ca/Si ratio C-S-H present in C_3S or Portland cement pastes [1,27,46]. In cement-slag blends, as the slag loading is increased the fibrillar (linear, directional) morphology is gradually replaced by the foil-like morphology [1]. An example of foil-like C-S-H is shown in Fig. 8. The foil-like morphology appears to be more efficient at filling space without leaving large interconnected capillary pores; it seems likely that this change in morphology of Op C-S-H from fibrillar to foil-like is largely responsible for the improved durability performance possible with slag- and pozzolan-containing systems.

While the morphologies of C-S-H observed by direct imaging of ion-thinned sections in the TEM may be to some extent artefacts of specimen preparation, (1) the shape of AFt relicts embedded in C-S-H is consistent with the observed morphologies being a good representation of the true morphologies [2], and (2) the C-S-H morphologies are very similar to those observed by TEM examination of replicas of fracture surfaces, which provide an image of the specimen totally without contact with vacuum or electron beam [45].

3.2. Chemical composition of C-S-H

Many compositional data for C-S-H in hardened cement pastes reported in the literature have been determined from energy dispersive X-ray analyses in an SEM (for example [47]). Because the X-ray generation volume in an SEM is

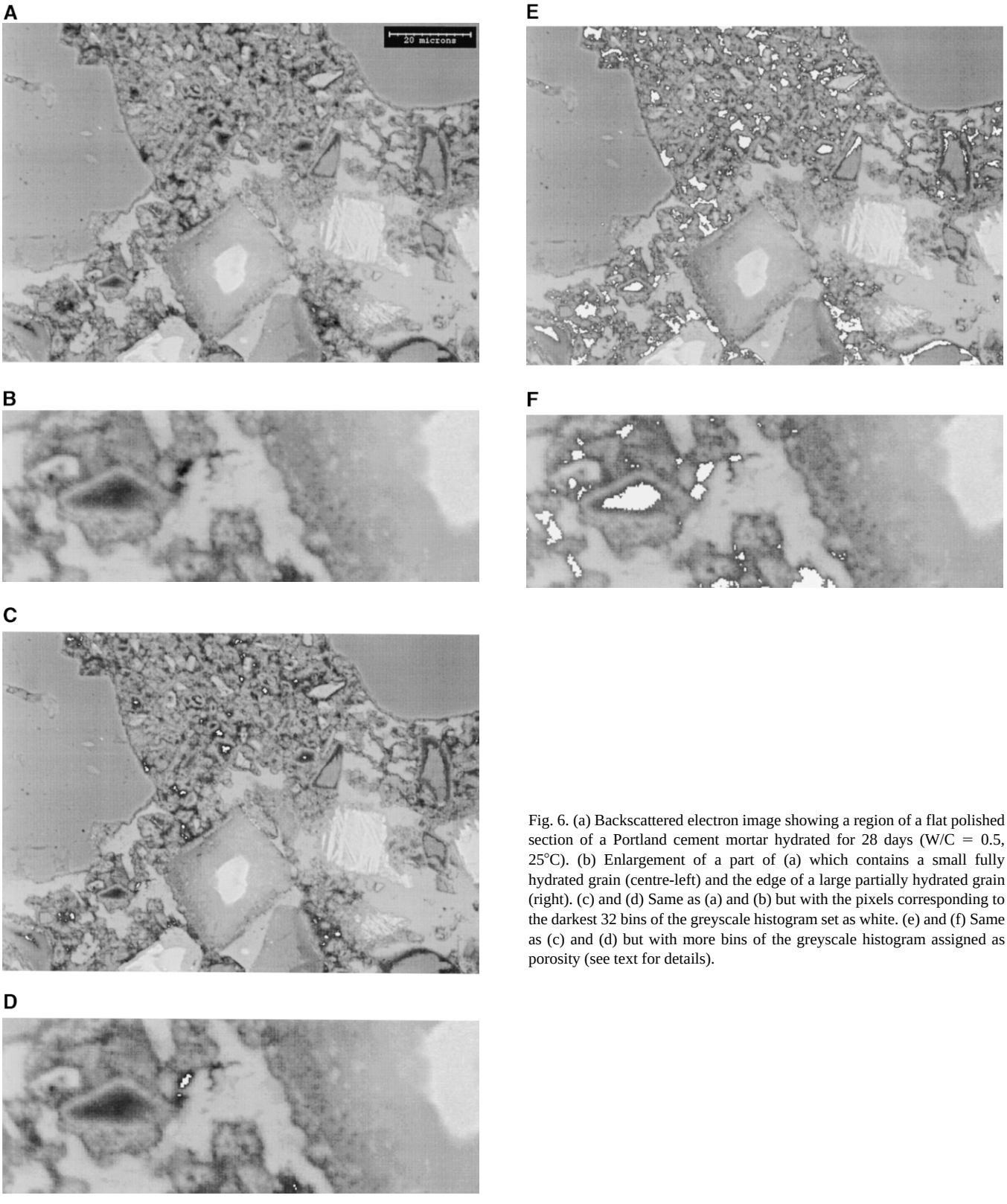

Fig. 6. (a) Backscattered electron image showing a region of a flat polished section of a Portland cement mortar hydrated for 28 days (W/C = 0.5, 25°C). (b) Enlargement of a part of (a) which contains a small fully hydrated grain (centre-left) and the edge of a large partially hydrated grain (right). (c) and (d) Same as (a) and (b) but with the pixels corresponding to the darkest 32 bins of the greyscale histogram set as white. (e) and (f) Same as (c) and (d) but with more bins of the greyscale histogram assigned as porosity (see text for details).

relatively large (several μm^3), the composition of C-S-H can often only be estimated after considering contributions from other phases intimately admixed with the C-S-H (for example [30,47,48]). This is not necessary with the higher resolution technique of TEM, where C-S-H can be analysed free of admixture with other phases [29]. Fig. 9 shows a Ca/Si ratio frequency histogram for X-ray microanalyses in the TEM of C-S-H present in hardened Portland cement pastes

Fig. 7. Transmission electron micrograph showing fine fibrillar Op C-S-H (top) and CH in a mature Portland cement paste.

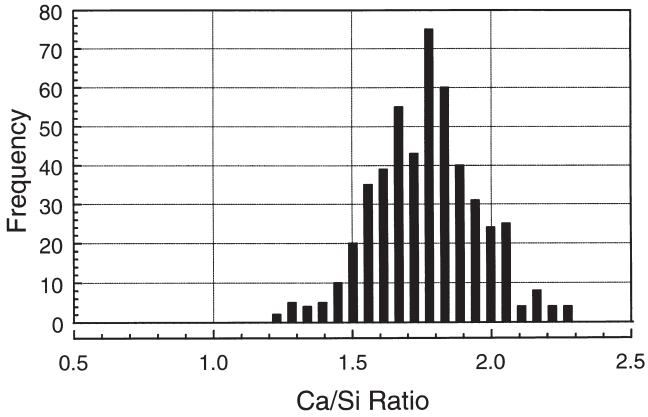

Fig. 9. Ca/Si ratio frequency histogram for C-S-H in Portland cement pastes aged 1 day to 3 1/2 years (493 TEM microanalyses of C-S-H free of admixture with other phases).

aged 1 day to 3 1/2 years (data largely from [2]). This is a large set of data which illustrates the extent of compositional variation possible for C-S-H present in neat portland cement pastes (hydrated at 20°C; W/C=0.4): from a Ca/Si ratio of ~1.2 to ~2.3 with a mean of ~1.75. It should be noted that the distributions vary with age: C-S-H present in young Portland cement pastes displays a bimodal Ca/Si ratio distribution which becomes unimodal with age [2]. Ip C-S-H generally has a higher mean Ca/Si ratio than Op [2]; reports of the opposite using analysis in the SEM [47,48,49] can probably be attributed to admixture with other phases.

Microanalysis in the TEM [1,26] has shown that in Portland cement-slag blends the composition of C-S-H changes as the proportion of slag is increased, the Al/Ca ratio increasing linearly with increasing Si/Ca ratio according to Eq. (1) [3,50],

$$\mathrm{Si/Ca} = 0.4277 + (2.366 \times \mathrm{Al/Ca}) \quad r^2 = 0.98 \qquad (1)$$

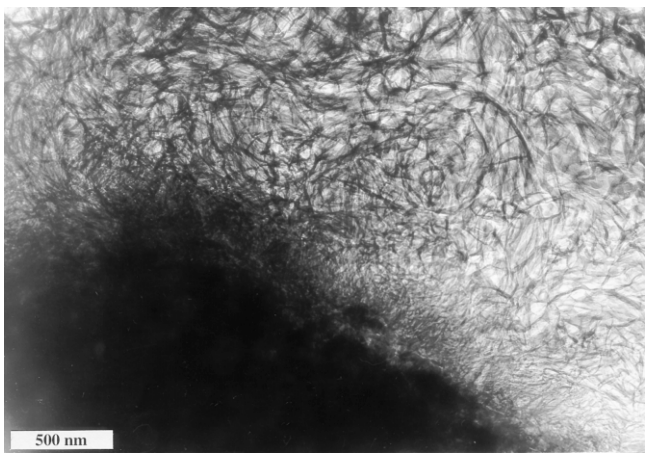

Fig. 8. Transmission electron micrograph showing foil-like Op C-S-H in a water-activated slag paste hydrated for 3 1/2 years at 40°C (W/S = 0.4).

This trend is confirmed by results from elemental mapping in an electron microprobe. Fig. 10 shows two scatter graphs from EMPA data for 50% cement 50% slag cement blends, aged 4 weeks and 14 months. Eq. (1), derived from analyses in the TEM of Op C-S-H free of admixture with other phases, is represented as the solid line in Fig. 10. Both regions were dominated by alite grains, either partially (4 weeks) or fully (14 months) hydrated. The bulk of the data points—corresponding to alite Ip—fall close to the trend line. Data for other cement-slag blends containing 10, 50, 83, and 90% slag, which also fall close to the trend line, are given elsewhere [41]. This linear trend suggests that there is a structural limitation on the incorporation of Al into C-S-H; Richardson and Groves assumed that Al is confined to the "bridging" sites of dreierkette-based silicate chains [50]. Fig. 11 shows a Ca/(Si+Al) frequency histogram incorporating 1186 individual TEM microanalyses of C-S-H present in a wide range of water-activated cement-slag systems (containing from 0→100% slag; see Table 1 for details). This figure illustrates the range of composition possible for C-S-H phases in Portland cement-slag systems: it is significant that there are very few analyses with Ca/(Si+Al) less than 0.83 or greater than 2.25 (the minimum and maximum values in Taylor's model for the structure of C-S-H [51]) with no analyses <0.67 or >2.5 (the minimum and maximum values in Richardson and Groves' model [52]).

3.3. Nanostructure of C-S-H

Much information has been gained in recent years on the nanostructure of C-S-H in hardened cements, principally from the techniques of trimethylsilylation (TMS) and solid-state nuclear magnetic resonance (NMR) spectroscopy. The two techniques are complementary: TMS gives semi-quantitative data on the fractions of Si present in different anionic species [33], whilst ^{29}Si NMR gives quantitative data on the fractions of Si present in silicate tetrahedra with different connectivities. Both techniques have shown that dimeric sili-

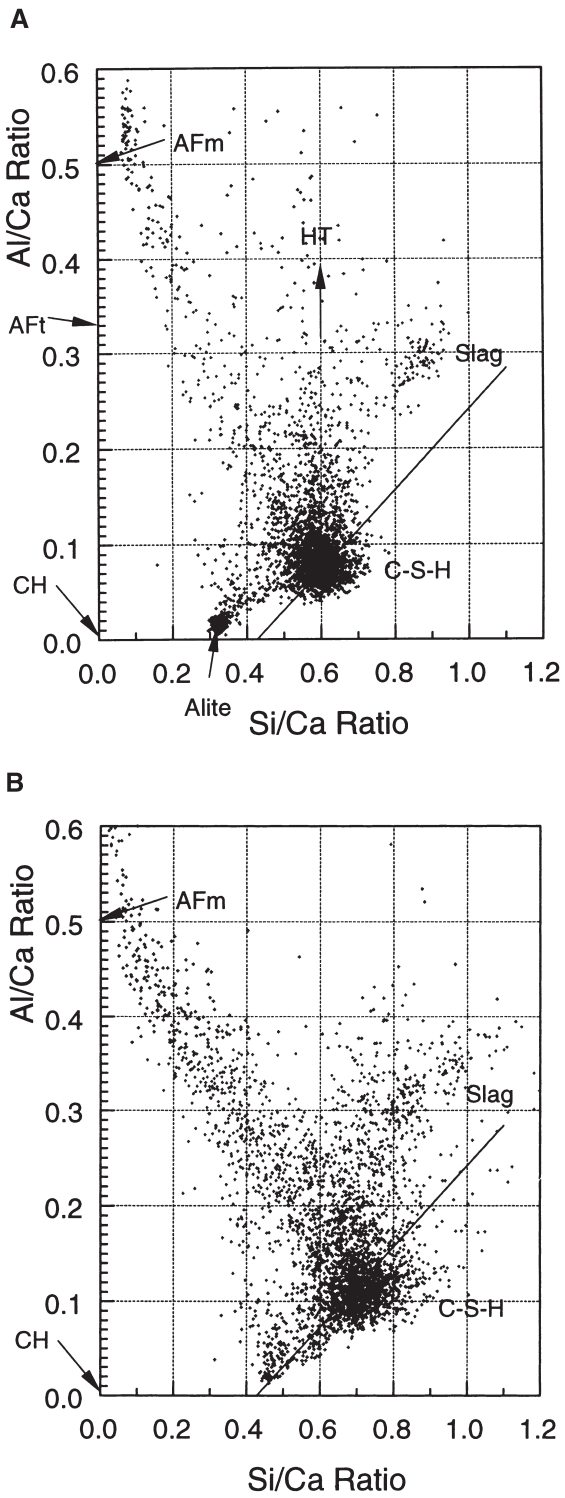

Fig. 10. (a) Al/Ca against Si/Ca atom ratio plot for the EMPA mapping data of an area (56 × 56 μm; 1-μm increments; 3136 analyses) in a 50% Portland cement 50% slag paste hydrated for 4 weeks. (b) Al/Ca against Si/Ca atom ratio plot for the EMPA mapping data of an area (58 × 60 μm; 1-μm increments; 3480 analyses) in a 50% Portland cement 50% slag paste hydrated for 14 months.

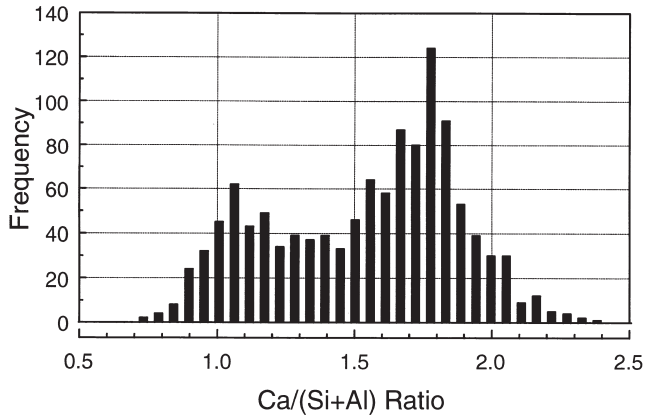

Fig. 11. Ca/(Si+Al) ratio frequency histogram for C-S-H in a wide range of water-activated cement-slag systems (0–100% slag). The plot includes 1186 individual TEM microanalyses of C-S-H free of admixture with other phases. System details are given in Table 1.

cate species predominate in the C-S-H formed during the first 24 hours after mixing C_3S, β-C_2S, or Portland cement pastes (W/C=0.4→0.5; 15→25°C) [53–58]. TMS has shown that the C-S-H formed subsequently consists of both dimeric and higher polymeric species, mainly linear pentamer and octamer, suggesting a 2,5,8 . . . (3*n*-1) sequence of linear silicate chain lengths [56–58]. In C_3S pastes the proportion of dimer passes through a maximum at ∼6 months but remains at ∼40% even after prolonged curing [57]: the distribution

Table 1
Breakdown of TEM microanalyses contributing to Fig. 11

Slag [6]	%	Cement/ activator	%	W/S	Temp. (°C)	Age	No. of analyses
–	–	β-C_2S	100	0.4	20	1 m	26
–	–	C_3S	100	0.4	20	3 1/2 y	68
–	–	C_3S	100	0.4	20	26 y	31
–	–	OPC	100	0.4	20	1 d	32
						1w	51
						3 m	39
						1 y	274
						2 y	46
						3 1/2 y	51
SC	10	OPC	90	0.4	20	14 m	18
SC	25	OPC	75	0.4	20	14 m	26
VL	50	WPC	50	0.4	25	3 w	48
SC	50	OPC	50	0.4	20	3 m	25
SC	50	OPC	50	0.4	20	14 m	35
SC	50	C_3S	50	0.4	20	1 m	51
SC	50	C_3S	50	0.4	60	1 m	46
SC	67	OPC	33	0.4	20	14 m	26
SC	75	OPC	25	0.4	20	14 m	21
SC	83	OPC	17	0.4	20	14 m	22
VL	90	WPC	10	0.4	25	3 w	25
SC	90	OPC	10	0.4	20	14 m	36
SC	90	C_3S	10	0.4	20	18 m	49
SC	100	–	–	0.4	20	12 m	30
						14 m	26
					40	3 1/2 y	44
SC	80	$Ca(OH)_2$	20	0.4	20	3 1/2 y	22
SC	80	$Ca(OH)_2$	15	0.4	20	14 m	18
		Gypsum	5				

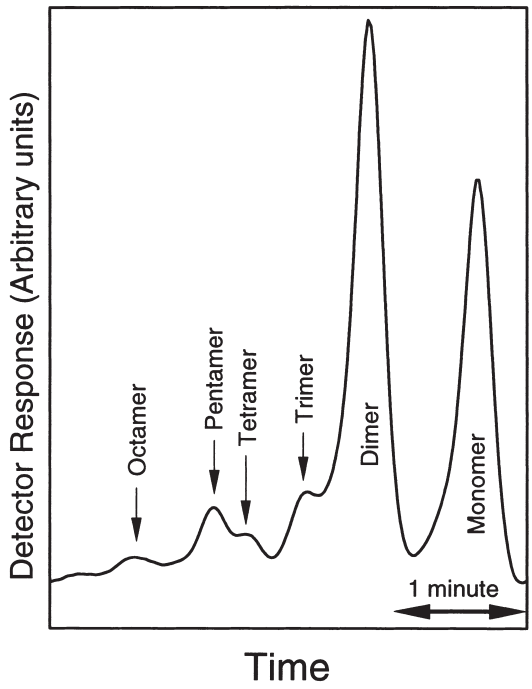

Fig. 12. TMS-GPC chromatogram of a white Portland cement paste hydrated for 3 months at 20°C; W/C = 0.55.

of anion sizes in the higher polymer fractions of C_3S and Portland cement pastes are essentially the same [57]. The type of data obtained from the two techniques are illustrated on Figs. 12 and 13, which show respectively trimethylsilyla-

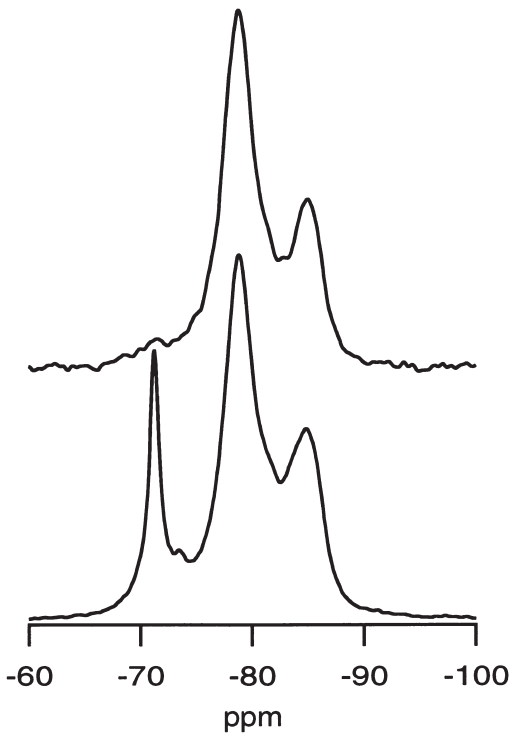

Fig. 13. ^{29}Si SP (bottom) and ^{1}H-^{29}Si CP MAS NMR spectra of a white Portland cement paste hydrated for 5 months at 25°C; W/C = 0.4.

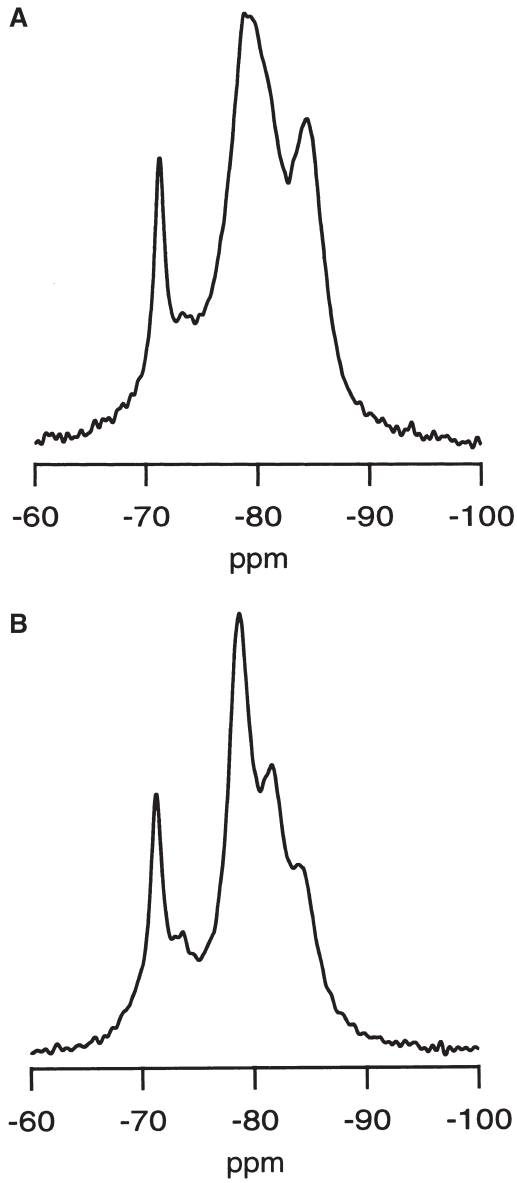

Fig. 14. (a) Single-pulse ^{29}Si NMR spectrum for a water-activated 50% white Portland cement 50% slag blend hydrated for 5 months at 25°C; W/S = 0.4. (b) Single-pulse ^{29}Si NMR spectrum for a 5*M* KOH-activated 50% white Portland cement 50% slag blend hydrated for 5 months at 25°C; S/S = 0.4.

tion-gel permeation chromatography (TMS-GPC) and ^{29}Si MAS NMR data for hydrated white cement pastes. The monomer on Fig. 12 is due principally to unreacted belite, although the ^{1}H-^{29}Si CP MAS NMR spectrum, Fig. 13 (top) indicates a small amount of hydrated monomer as a reaction product, consistent with the data of Clayden et al. and Rodger et al. [59,60]. Dimer is the predominant silicate species in the C-S-H, with linear pentamer as the next most abundant, with some linear octamer. The trimer and tetramer labelled on Fig. 12 have been attributed to side-reactions [10]. ^{29}Si MAS NMR can provide quantitative information on the fractions of silicon present in different tetrahedral environments, Q^n ($0 \leqslant n \leqslant 4$), where Q is a silicate tetrahedron

and *n* is the number of oxygens which bridge to adjacent tetrahedra. On the ^{29}Si single pulse spectrum of Fig. 13 (bottom), the peak at −71.3 ppm is due to unreacted belite (Q^0), and the broader peaks at −79 and −85 ppm are due respectively to end- (Q^1) and middle-chain (Q^2) groups present in the C-S-H [61]. An average chain length can be calculated from the ^{29}Si single pulse data from Eq. (2):

$$\overline{CL} = \frac{2}{\left(\frac{Q^1}{Q^1 + Q^2}\right)}. \quad (2)$$

In cement-slag blends, the C-S-H also contains Al—the Al/Ca ratio varying with Si/Ca ratio according to Eq. (1)—and this will affect the NMR spectra [62,63]. In alumino-silicates the characteristic up-field chemical shifts caused by the increased polymerization of the Q^n building units are further influenced by the replacement of Si by Al. There are 15 possible $Q^n(m\text{Al})$ structural units where Q is a silicate tetrahedron connected via oxygen bridges to *m* Al and *n-m* other Si atoms, with $n=0$ to 4 and $m=0$ to *n*. Fig. 14(a) shows the ^{29}Si single pulse NMR spectrum for a 50% white Portland cement 50% slag blend hydrated for 5 months at 25°C (W/S = 0.4). As with the neat Portland cement spectrum, Fig. 13 (bottom), the sharp peak at −71.3 ppm is due to unreacted belite; there is also a contribution from unreacted slag (a broad peak centred at around −73 ppm [27,64]). There appear to be three hydrate peaks, but more information is needed to deconvolute the spectrum. Such information can be obtained by activating the blends with 5*M* KOH solution [3]: the hydration products and microstructures obtained by alkali activation are similar to water activation with the difference that the CH is microcrystalline and the C-S-H is structurally better ordered, resulting in narrower NMR linewidths and so improved resolution. This is illustrated in Fig. 14(b), which again shows a spectrum for a 50% cement 50% slag blend but in this case activated with 5*M* KOH solution. The hydrate peaks in this spectrum are very clearly defined and the results from its deconvolution can be used to aid deconvolution of the spectrum from the water-activated paste. Richardson and Groves [3] reported results for cement-slag blends containing 50 and 90% slag. As for C_3S and neat cement systems, peaks at ∼−79 ppm and ∼−85 ppm were attributed to Q^1 and Q^2 species respectively. A peak at ∼-82 ppm was assigned as Q^2(1Al), consistent with the assignment of peaks at similar positions in the ^{29}Si NMR spectra of Al-substituted tobermorites [65,66]. The average Al/Si ratios for the C-S-H—calculated from the deconvoluted peak areas using Eq. (3)—were in excellent agreement with those measured directly in the TEM, thus supporting strongly the assignment of the peaks and the assumption that Al was not present in chain-terminating tetrahedra.

$$Al/Si = \frac{\frac{1}{2}Q^2(1Al)}{Q^1 + Q^2(0Al) + Q^2(1Al)} \quad (3)$$

The average chain lengths were calculated using Eq. (4):

$$\overline{CL} = \frac{2}{\left(\frac{Q^1}{Q^1 + Q^2(0Al) + \frac{3}{2}Q^2(1Al)}\right)}. \quad (4)$$

The assignment of the peak at ∼−82 ppm solely to Q^2(1Al) followed earlier work on the location of Al in semi-crystalline C-S-H phases formed by the reaction of a slag and a synthetic slag glass activated by 5*M* KOH solution [27,67]:

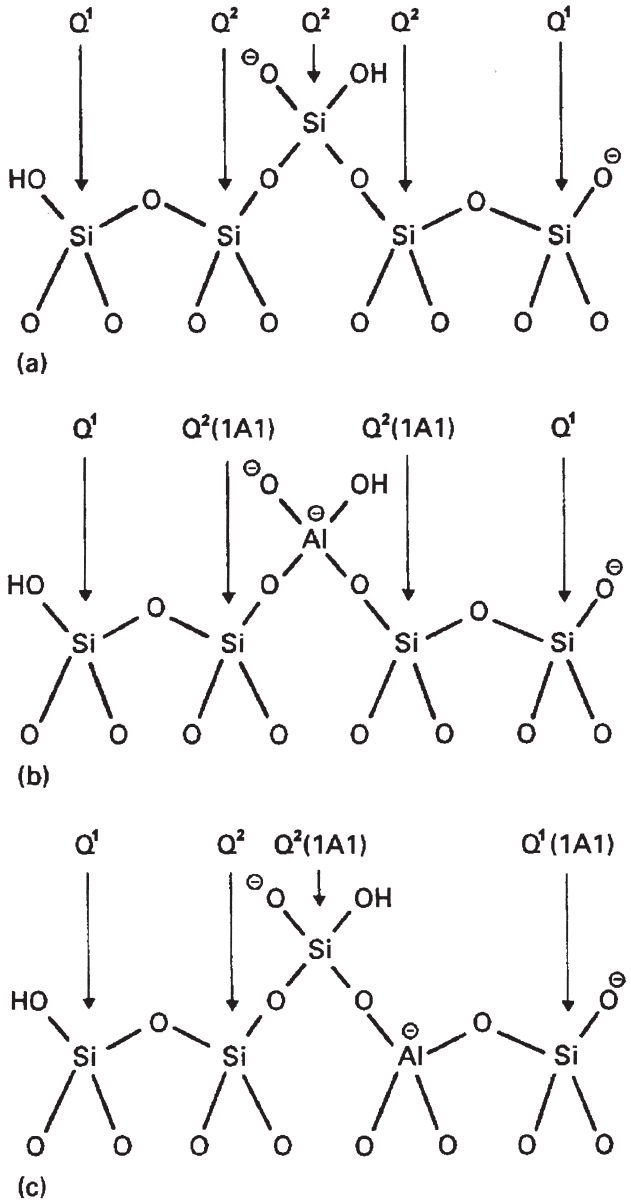

Fig. 15. (a) Schematic representation of a pentameric silicate chain of the type present in dreierkette-based models for the structure of C-S-H. Q^1 and Q^2 units are identified; the middle Q^2 unit is the 'bridging' tetrahedron. (b) The same as (a), but with Al^{3+} substituted for Si^{4+} in the bridging tetrahedron. (c) The same as (a), but with Al^{3+} substituted for Si^{4+} in a non-bridging tetrahedron.

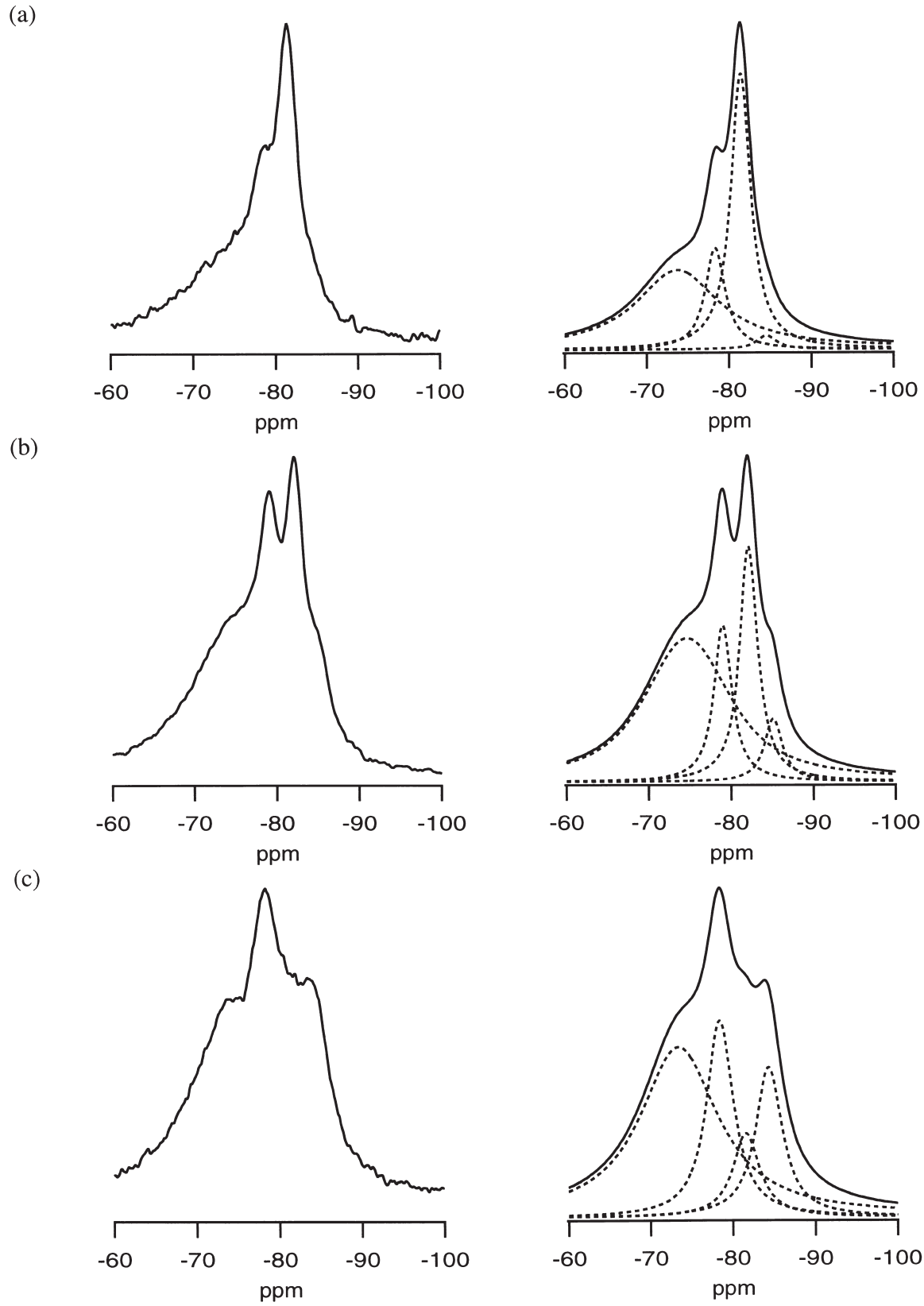

Fig. 16. Single-pulse ^{29}Si NMR spectra (left) and fits (right) for three 5*M* KOH-activated slags (hydrated for 7 days at 20°C, S/S = 0.4) with (a) high Al content, (b) intermediate Al content, and (c) low Al content.

the single pulse ^{29}Si and ^{1}H-^{29}Si CP MAS NMR spectra gave conclusive evidence that Al substituted for Si only in the central tetrahedron of pentameric silicate chains (or in every third tetrahedron in octameric chains). The data were interpreted in terms of a dreierkette model for the structure of C-S-H, as illustrated in Fig. 15. Since there were no Q^1(1Al) units (chemical shift ≈ -75 ppm) on the ^{29}Si CP MAS NMR spectra Al could—assuming no chain-terminating Al—only be substituted for Si in "bridging" tetrahedra (see Fig. 15); Q^1(1Al) units would be expected if Al substituted for Si at non-bridging sites. There could not have been significant numbers of chain-terminating Al because there was good agreement between the Al/Si ratios derived from NMR and analytical TEM [27,67]; chain-terminating Al would have produced higher Al/Si ratios from NMR than from TEM, which gives compositions for C-S-H free of admixture with other phases.

The association of the peak at ~ -82 ppm with Al is well-illustrated by Fig. 16 which shows ^{29}Si SP MAS NMR spectra for three KOH-activated slags with high, intermediate and low Al contents. In the slag with high Al/Si, the peak at -82 ppm is very prominent—in fact, assuming the above assignment of peaks, the bridging sites of the C-S-H structure would be almost saturated with Al—and it becomes markedly less prominent with reduced Al/Si ratio. Results of deconvolution of the spectra are: (a) high Al content (Al/Si of anhydrous slag = 0.62) Al/Si of C-S-H = 0.34, $\overline{CL}$ = 9.8, % hydration = 53; (b) intermediate Al content (Al/Si of anhydrous slag = 0.36) Al/Si of C-S-H = 0.25, $\overline{CL}$ = 7.3, % hydration = 42; and (c) low Al content (Al/Si of anhydrous slag = 0.17) Al/Si of C-S-H = 0.11, $\overline{CL}$ = 5.2, % hydration = 45. The Al/Si and $\overline{CL}$ of the C-S-H were calculated using Eqs. (3) and (4). Spectra similar to that for the intermediate Al-content slag have been published previously for activation with KOH [27] and NaOH [68] solutions. The excellent agreement between the Al/Si ratios derived from the deconvolution of NMR spectra and from microanalysis in the TEM for a range of systems is illustrated on Fig. 17. Despite these data, the assignment of the peaks at ~ -79 ppm, ~ -82 ppm and ~ -85 ppm to Q^1, Q^2(1Al) and Q^2 species respectively has been questioned recently by Faucon et al. [69,70,71]. In studies on synthetic C-S-H phases, they suggested that Al could also enter non-bridging tetrahedra, especially in C-S-H with higher Ca/Si ratios. It is possible to test Faucon et al.'s assertion using trimethylsilylation since from its standpoint substituents are not part of the silicate anions [33]. If Al substituted solely at bridging sites then the 3*n*-1 sequence of chain lengths would be maintained: a C-S-H with its bridging sites saturated with Al would give just dimeric derivatives. Substitution at bridging *and* non-bridging sites would produce enhanced amounts of trimer and tetramer (enhanced because some trimer and tetramer are produced by side reactions [10]).

Fig. 18 shows the TMS-GPC data for a 50% white cement 50% slag blend activated with 5*M* KOH solution, similar to that reported in [3] in which the C-S-H had Ca/Si $\approx$ 1.55 and Al/Si $\approx$ 0.13. The monomer is due to unreacted belite and slag-glass; the slag-glass may also have contributed a very small amount of dimer and trimer [64]. The predominant derivative is dimer, with the curve consistent with the 3*n*-1 sequence of chain lengths. Since there is no enhancement of the proportions of trimer and tetramer compared with the neat white cement paste, Fig. 12, the data support the view that Al substitute for Si solely at bridging sites.

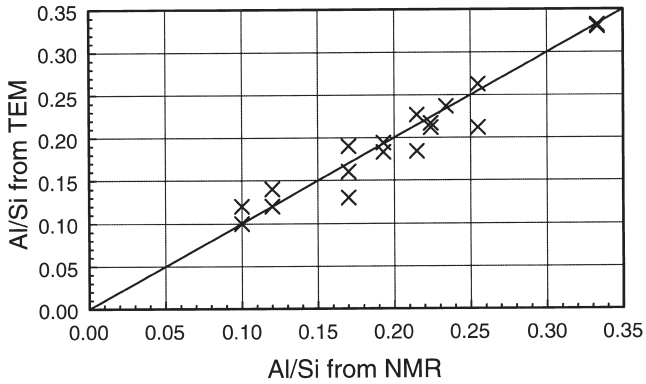

Fig. 17. Plot of Al/Si ratio of C-S-H measured directly in the TEM against Al/Si ratio calculated from NMR spectra for a range of slag-containing cement pastes; details of the systems are given in [6].

Fig. 19 shows the TMS-GPC data for a synthetic slag glass activated with 5*M* KOH solution, similar to that reported in [67] in which the C-S-H had a Ca/Si $\approx$ 1.10 and Al/Si $\approx$ 0.21. The data are very similar to the neat cement

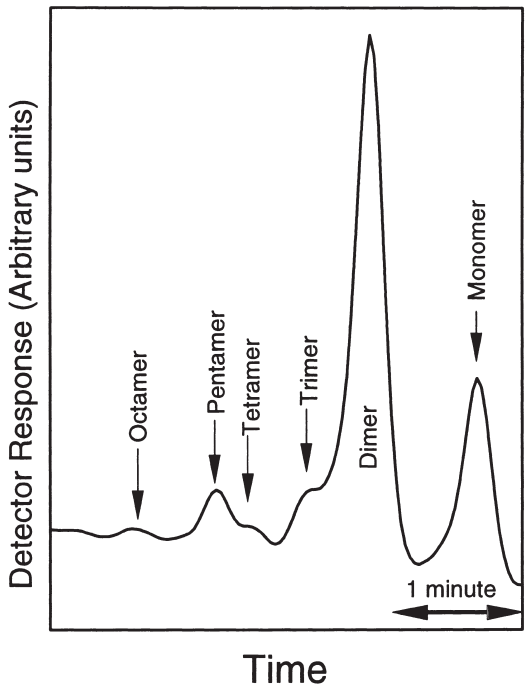

Fig. 18. TMS-GPC chromatogram of a KOH-activated 50% white Portland cement 50% slag paste hydrated for 5 1/4 years at 20°C; S/S = 0.5.

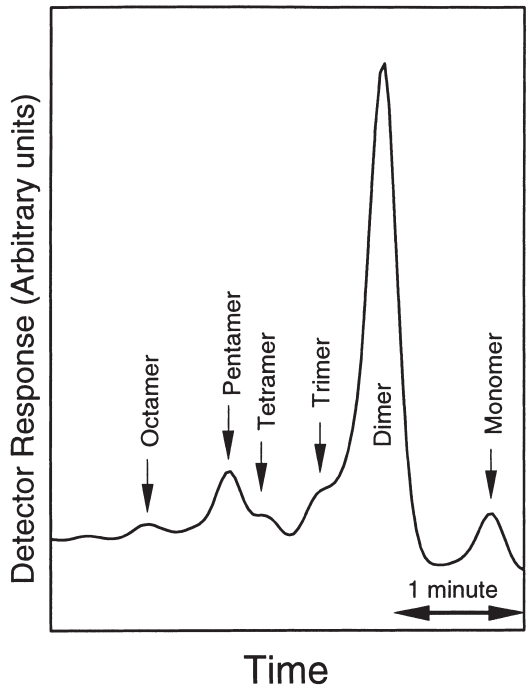

Fig. 19. TMS-GPC chromatogram of a KOH-activated synthetic slag glass hydrated for 5 3/4 years at 20°C; S/S = 0.4.

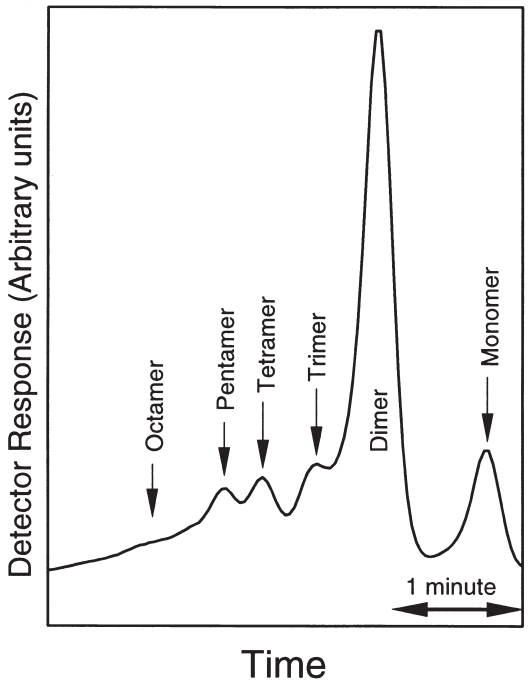

Fig. 20. TMS-GPC chromatogram of a KOH-activated slag with high Al content hydrated for 2 1/4 years at 20°C; S/S = 0.4.

paste, Fig. 12, despite the much higher Al/Si ratio: again, the data support the view that Al substitute for Si solely at bridging sites since there is no enhancement of the proportions of trimer and tetramer. Microanalysis in the TEM of the C-S-H present in the 5*M* KOH-activated slag system with high Al/Si ratio—the NMR spectrum of which is given in Fig. 16 for 7 days hydration—shows that it has a very high Al content (Al/Si ≈ 0.33, Ca/Si ≈ 1.10). Assignment of the peaks on Fig. 16 at ∼−79 ppm, ∼−82 ppm, and ∼−85 ppm solely to Q^1, Q^2(1Al), and Q^2 species, respectively, would mean that the bridging sites were almost saturated with Al. The large amount of dimer on the TMS-GPC curve, Fig. 20, confirms this conclusion.

In all the above three cases—including the higher Ca/Si ratio blend system—the TMS-GPC data are consistent with the 3*n*-1 sequence of chain lengths with dimer as the predominant species: the data show unequivocally that the C-S-H in these hardened cements contain Al substituted for Si solely at bridging sites. The data support strongly the assignment of the peaks on the ^{29}Si NMR spectra at ∼−79 ppm, ∼−82 ppm, and ∼−85 ppm solely to Q^1, Q^2(1Al), and Q^2 species, respectively.

The approach adopted in [3] for cement-slag blends can also be used for Portland cement blends containing other mineral additions. Figs. 21 and 22 show ^{29}Si MAS NMR spectra for blends of white cement with fly ash (30%) and metakaolin (20%). On Fig. 21 the broad peak at ∼−105 ppm is due to unreacted fly-ash. The unreacted metakaolin gave a very broad peak at ∼−100 ppm. The spectra for the water-activated pastes are very similar to those for blends containing slag, Fig. 14(a) and [3]. Again, the hydrate peaks in the KOH-activated spectra are clearly defined and the results from the deconvolution of these spectra can be used to aid deconvolution of the water-activated spectra. TMS-GPC data again show that Al substitutes for Si solely at bridging sites because the observed chain lengths follow the 3*n*-1 sequence, for example Figs. 23 and 24; there is no significant enhancement of the proportions of trimer and tetramer compared with the neat white cement paste, Fig. 12. Any unreacted pozzolan would make no (fly ash [64]) or only a very minor (metakaolin [72]) contribution to the TMS-GPC data. The C-S-H in the KOH-activated metakaolin system, Fig. 22, is similar to that present in the high Al content slag (Fig. 16); the alumino-silicate chains are on average very long and the bridging sites are nearly saturated with Al which leads to predominantly dimeric TMS derivatives. The hydration products and microstructure of the fly ash and metakaolin blended systems are discussed in greater detail elsewhere [4].

The C-S-H phases in all the systems discussed in this paper can be described by Richardson and Groves' dreierkette-based model for the structure of substituted C-S-H [50], which can be represented by formula (5):

$$\{Ca_{2n}H_w(Si_{1-a}R_a^{[4]})_{(3n-1)}O_{(9n-2)}\}\cdot I^{c+}_{\frac{a}{c}(3n-1)}\cdot (OH)_{w+n(y-2)}\cdot Ca_{\frac{n\cdot y}{2}}\cdot mH_2O \quad (5)$$

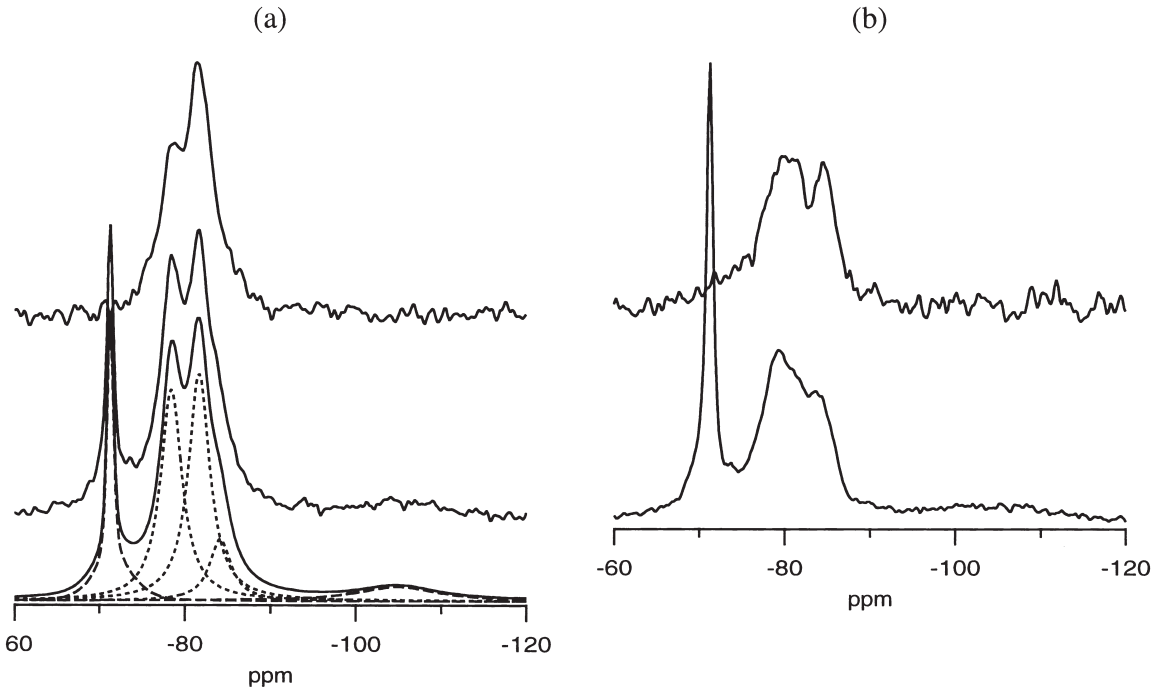

Fig. 21. Single pulse ^{29}Si (bottom) and ^{1}H-^{29}Si CP MAS NMR spectra of (a) KOH-activated and (b) water-activated 70% white Portland cement 30% fly ash pastes hydrated for 4 months at 25°C; S/S = 0.5.

where $R^{[4]}$ is a trivalent cation, mainly Al^{3+}, in tetrahedral co-ordination and I^{c+} is an interlayer ion, either a monovalent alkali cation or Ca^{2+}, charge-balancing the R^{3+} substitution for Si^{4+}. Since Al substitutes for Si solely in the bridging tetrahedra of the dreierkette structure, and there are *n*-1 bridging sites [Eq. (6)],

$$0 \leqslant a \leqslant \frac{n-1}{3n-1}. \tag{6}$$

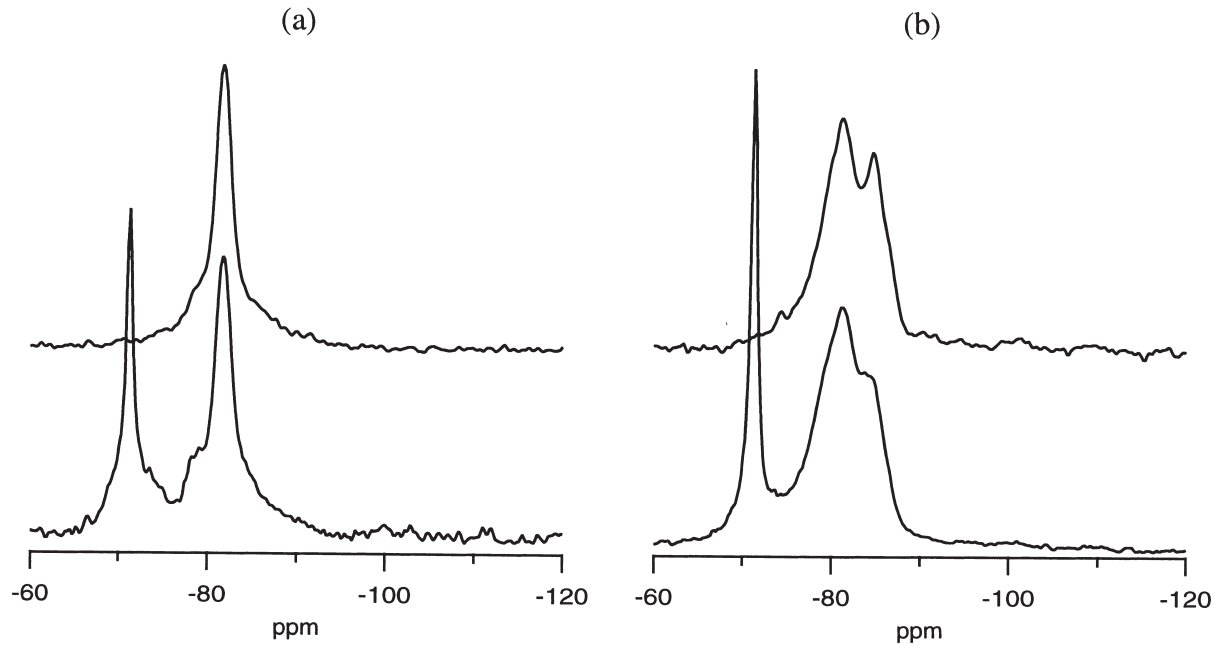

Fig. 22. Single pulse ^{29}Si (bottom) and ^{1}H-^{29}Si CP MAS NMR spectra of (a) KOH-activated and (b) water-activated 80% white Portland cement 20% metakaolin pastes hydrated for 4 months at 25°C; S/S = 0.55.

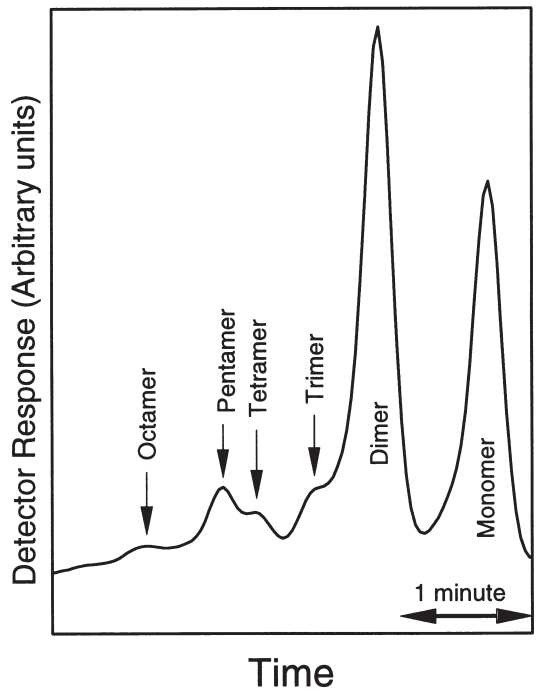

Fig. 23. TMS-GPC chromatogram of a KOH-activated 70% white Portland cement 30% fly ash paste hydrated for 7 months at 20°C; S/S = 0.5.

The model, and the limits placed on the variables, are discussed in detail elsewhere [50,52].

3.4. The bonding of C-S-H to other phases

The strength of hardened Portland cement pastes depends in part on the ability of the C-S-H to bond effectively

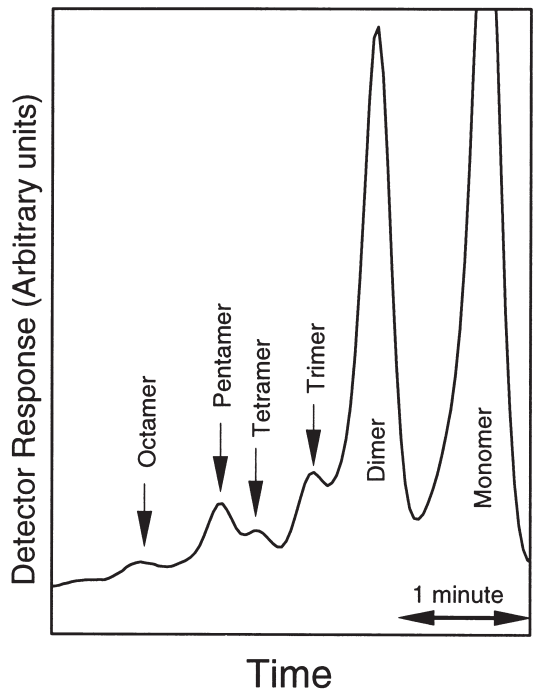

Fig. 24. TMS-GPC chromatogram of a water-activated 80% white Portland cement 20% metakaolin paste hydrated for 3 months at 20°C; W/S = 0.55.

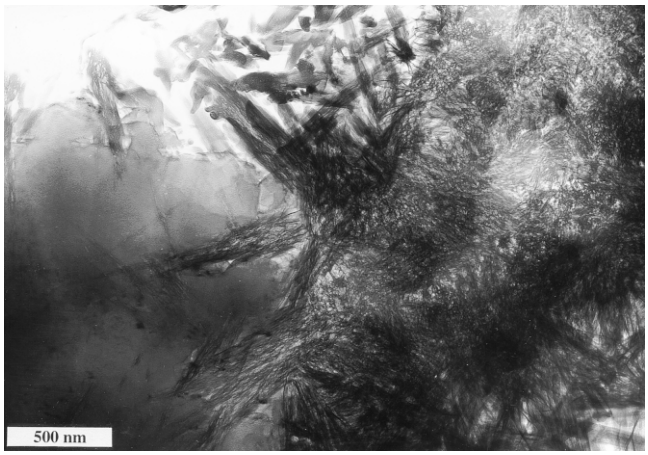

Fig. 25. Transmission electron micrograph showing fibrillar Op C-S-H well-bonded with CH in a C_3S paste hydrated for 3 1/2 years at 20°C (W/C = 0.4).

to other products of hydration, most notably to calcium hydroxide. CH generally occurs as massive crystals but is also admixed with C-S-H at the micron-scale. Bonding with Op C-S-H is often excellent [2,20], as illustrated in Fig. 25, but is less-good where the interface is parallel to the basal plane of the CH. In such cases, the fine-fibrillar Op C-S-H bonds to a thin layer of C-S-H which tends to form along the crystal surface, as in Fig. 7 [2,20]. Where the two make contact the bond between CH and Ip C-S-H is very good [2,20].

Intimate nanoscale mixtures of C-S-H and microcrystalline CH have been observed in cements with very low water:cement ratio [73], in pozzolanic cements [74], and in Portland cements activated with KOH solution [3].

Another example of nanoscale mixture of C-S-H with a crystalline phase is found in the slag Ip of slag-containing cements. As noted in section 3.1.2, Ip from larger slag grains commonly displays the typical compact fine-scale homogeneous morphology, but it is chemically distinct in having high content of Mg and Al. Laths or platelets are also often observed which are particularly rich in Mg and Al. Microanalysis in both EMPA and TEM of slag Ip in a range of systems has shown a linear relationship between the increase in Mg/Ca ratio and Al/Ca ratio [1,3,27], with the Al/Ca ratio at Mg/Ca = 0 similar to that of the Op C-S-H. This relationship is due to different levels of admixture within the analysed volume of a single-phase C-S-H compositionally equivalent to Op C-S-H (with any Al as $Al^{[4]}$) and a Mg,Al-rich hydroxide phase (with $Al^{[6]}$) [50,67,75], and the generalized formula [Eq. (7)]:

$$[R^{2+}_{1-k}R^{3+}_{k}(OH)_2]^{k+} \cdot R^{r-}_{\frac{k}{r}} \cdot jH_2O \qquad (7)$$

where $R^{2+} = Mg^{2+}$; $R^{3+} = Al^{3+}$ or Fe^{3+}; and $R^{r-} = OH^-$, SO_4^{2-}, CO_3^{2-}. For hydrotalcite-like phases in general $\sim 0.2 \leqslant k \leqslant 0.33$ [76,77], whilst in slag-containing cements k is typically ~ 0.3 [1,6].

A strong mutual attraction between the main layers of

Al-substituted C-S-H and the Mg,Al-hydroxide phase due their opposite charges [see Eqs. (5) and (7)] might be an explanation for the very fine level of admixture present in the Ip regions with the homogeneous morphology, such as that illustrated in Fig. 4 [78]. It is certainly true that Ip with this morphology is more common in those systems with the greatest level of Al substitution for Si in the C-S-H, with fewer well-defined platelets. A similar explanation has been given to account for the apparent ability of C-S-H to destroy AFm phases [33] (in formula (7), AFm phases have R^{2+} = Ca; R^{3+} = Al^{3+} or Fe^{3+}; R^{r-} = OH^-, SO_4^{2-}, CO_3^{2-}, or other common anions; *k* has a fixed value of 0.33).

4. Conclusions

1. Taplin's [11] long-standing "inner-outer" classification of the products of cement hydration is supported strongly by the high resolution technique of transmission electron microscopy of ion-thinned sections. The more recent "phenograin-groundmass" classification due to Diamond and Bonen [31] would seem to have little application outside the description of backscattered electron images.
2. Ip C-S-H present in larger Portland cement grains typically has a fine-scale and homogeneous morphology with pores somewhat under 10 nm in diameter. This product is very unstable in the electron beam in the TEM making work at higher magnifications difficult. Ip from larger slag grains also displays this morphology, but is chemically distinct in having high content of Mg and Al.
3. TEM shows that the hydrated remains of small particles—whether of Portland cement, slag, or fly ash—contain a less dense product with substantial porosity surrounded by a zone of relatively dense C-S-H. This has implications for the analysis of porosity and pore-size distributions on backscattered electron images.
4. In cement-slag blends, the fibrillar morphology of Op C-S-H is gradually replaced by a foil-like morphology as the slag loading is increased. It seems likely that this change in morphology is largely responsible for the improved durability performance possible with slag-containing systems.
5. The Ca/Si ratio of C-S-H in neat Portland cement pastes varies from ~1.2 to ~2.3 with a mean of ~1.75.
6. The Ca/(Si+Al) ratio of C-S-H in water activated cement-slag pastes (0–100% slag) varies from ~0.7 to ~2.4; these limits are consistent with dreierkette-based models for the structure of C-S-H [51,52].
7. Al substitutes for Si in C-S-H only in the "bridging" tetrahedra of dreierkette chains; this is true for a range of systems, including blends of Portland cement with slag, fly ash, and metakaolin. The C-S-H in these systems can be described by Richardson and Groves' model for the structure of substituted C-S-H [50].
8. The bonding of C-S-H to other products of hydration is generally good.

Acknowledgments

Thanks are due to the Engineering and Physical Sciences Research Council for funding under Grant Nos. GR/H64972, GR/K52089 and GR/K65478, to Dr Geoff. Groves and Prof. Joe Cabrera for encouragement and support, to Prof. Neville Boden (SOMS Centre, University of Leeds) and Prof. Chris Dobson FRS (Inorganic Chemistry Lab., University of Oxford) for provision of the NMR facilities, to Prof. J. Francis Young and Ms. Xiaofeng Zhu for the TMS work (Centre for Cement Composite Materials, University of Illinois, Urbana), to Dr Adrian Brough and Ms. Charlotte Famy (Imperial College, London) for the backscattered electron micrographs, to Mr Martin Head (School of Civil Engineering, University of Leeds) for the image analysis, and to Prof. Hal Taylor for valuable discussions.

References

[1] I.G. Richardson, G.W. Groves, The microstructure and microanalysis of hardened cement pastes involving ground granulated blast-furnace slag, J Mater Sci 27 (1992) 6204–6212.
[2] I.G. Richardson, G.W. Groves, The microstructure and microanalysis of hardened ordinary Portland cement pastes, J Mater Sci 28 (1993) 265–277.
[3] I.G. Richardson, G.W. Groves, The structure of the calcium silicate hydrate phases present in hardened pastes of white Portland cement/blast-furnace slag blends, J Mater Sci 32 (1997) 4793–4802.
[4] C. Love, I.G. Richardson, The microstructure and composition of blended cement pastes incorporating fly ash and metakaolin, to be submitted to Cem Concr Res.
[5] I.G. Richardson, C. Love, D.L. Ou, The microstructure and composition of alkali-activated slag cement pastes, to be submitted to Cem Concr Res.
[6] I.G. Richardson, The structure of C-S-H in hardened slag cement pastes, in: 10th International Cong Chemistry of Cement, 2 (1997) 2ii068, 8pp.
[7] G.W. Groves, P.J. LeSueur, W. Sinclair, Transmission electron microscopy and microanalytical studies of ion-beam-thinned sections of tricalcium silicate paste, J Am Ceram Soc 69 (1986) 353–356.
[8] J. Rocha, J. Klinowski, Kaolinite as a convenient standard for setting the Hartmann-Hahn match for ^{29}Si CP MAS NMR of silicates, J Magn Reson 90(3) (1990) 567–568.
[9] WaveMetrics, Inc., Igor (1992) and Igor Pro (1996), Lake Oswego, Oregon, 97035, USA. A.R. Brough, D.Phil. Thesis, University of Oxford, 1993.
[10] P. Lu, G. Sun, J.F. Young, Phase composition of hydrated DSP cement pastes, J Am Ceram Soc 76(4) (1993) 1003–1007.
[11] J.H. Taplin, A method for following the hydration reaction in Portland cement paste, Australian J Appl Sci 10 (1959) 329–345.
[12] R.B. Williamson, Solidification of Portland cement, Prog Mater Sci 15(3) (1972) 189–286.
[13] S. Diamond, Cement paste microstructure—an overview at several levels, in: Hydraulic cement pastes: Their structure and properties, Proceedings of a conference held at the University of Sheffield, 8–9th April 1976. Cement and Concrete Association, Slough, (1976) 2–30.
[14] S. Goto, M. Daimon, G. Hosaka, R. Kondo, Composition and morphology of hydrated tricalcium silicate, J Am Ceram Soc 59(7/8) (1976) 281–284.
[15] B.D. Barnes, S. Diamond, W.L. Dolch, Hollow shell hydration of cement particles in bulk cement paste, Cem Concr Res 8 (1978) 263–271.
[16] D.D. Double, An examination of the hydration of Portland cement by electron microscopy, Silicate Industriels 11 (1976) 233–246.
[17] P.L. Pratt, A. Ghose, Electron microscope studies of Portland cement microstructures during setting and hardening, Phil Trans R Soc Lond A310 (1983) 93–101.

[18] D.L. Rayment, E.E. Lachowski, The analysis of OPC pastes: A comparison between analytical electron microscopy and electron probe microanalysis, Cem Conc Res 14 (1984) 43–48.
[19] K.O. Kjellsen, H.M. Jennings, B. Lagerblad, Evidence of hollow-shells in the microstructure of cement paste, Cem Concr Res 26 (1996) 593–599.
[20] G.W. Groves, TEM studies of cement hydration, Mater Res Soc Symp Proc 85 (1987) 3–12.
[21] B.J. Dalgleish, K. Ibe, Thin-foil studies of hydrated cement, Cem Concr Res 11 (1981) 729–739.
[22] H.M. Jennings, B.J. Dalgleish, P.L. Pratt, Morphological development of hydrating tricalcium silicate as examined by electron microscopy techniques, J Am Ceram Soc 64 (1981) 567–572.
[23] S.A. Rodger, G.W. Groves, The microstructure of tricalcium silicate/ pulverized fuel ash blended cement pastes, Adv Cem Res 1(2) (1988) 84–91.
[24] S.A. Rodger, G.W. Groves, Electron microscopy study of ordinary Portland cement and ordinary Portland cement-pulverized fuel ash blended pastes, J Am Ceram Soc 72(6) (1989) 1037–1039.
[25] I.G. Richardson, S.A. Rodger, G.W. Groves, The porosity and pore structure of hydrated cement pastes as revealed by electron microscopy techniques, Mat Res Soc Symp Proc 137 (1989) 313–318.
[26] I.G. Richardson, S.A. Rodger, G.W. Groves, The microstructure of GGBFS/OPC hardened cement pastes and some effects of leaching, Mat Res Soc Symp Proc 176 (1990) 63–74.
[27] I.G. Richardson, A.R. Brough, G.W. Groves, C.M. Dobson, The characterization of hardened alkali-activated blast-furnace slag pastes and the nature of the calcium silicate hydrate (C-S-H) phase, Cem Concr Res 24 (1994) 813–829.
[28] D. Viehland, J.F. Li, L.J. Yuan, Z.K. Xu, Mesostructure of calcium silicate hydrate (C-S-H) gels in Portland-cement paste—short-range ordering, nanocrystallinity, and local compositional order, J Am Ceram Soc 79(7) (1996) 1731–1744.
[29] H.F.W. Taylor, Studies on the chemistry and microstructure of cement pastes, Proc Brit Ceram Soc 35 (1984) 65–82.
[30] H.F.W. Taylor, D.E. Newbury, An electron microprobe study of a mature cement paste, Cem Concr Res 14 (1984) 565–573.
[31] S. Diamond, D. Bonen, Microstructure of hardened cement paste—a new interpretation, J Am Ceram Soc 76(12) (1993) 2993–2999.
[32] H.F.W. Taylor, Cement Chemistry, Academic Press, 1st Ed., New York, 1990.
[33] H.F.W. Taylor, Cement Chemistry, 2nd Ed., Thomas Telford, London, 1997.
[34] A.J. Allen, C.G. Windsor, V. Rainey, D. Pearson, D.D. Double, N. McN Alford, A small angle neutron scattering study of cement porosities. J Phys D: Appl Phys 15 (1982) 1817–1833.
[35] D. Pearson, A.J. Allen, A study of ultrafine porosity in hydrated cements using small angle neutron scattering. J Mater Sci 20 (1985) 303–305.
[36] I.G. Richardson, The microstructure and composition of hardened cement pastes, D.Phil. Thesis, University of Oxford, 1991.
[37] D. Viehland, L.J. Yuan, Z. Xu, Structural studies of jennite and 1.4 nm tobermorite: disordered layering along [100] of jennite, J Am Ceram Soc 80 (12) (1997) 3021–3028.
[38] F.T. Ewart, F. Glasser, G. Groves, T. Jappy, R. McCrohan, P.T. Moseley, S. Rodger, I. Richardson, Mechanisms of sorption in the near field, AEA Technology Harwell, (1990) *AERE report R 13800.*
[39] Q.L. Feng, E.E. Lachowski, F.P. Glasser, Densification and migration of ions in blast furnace slag-Portland cement pastes, Mat Res Soc Symp Proc 137 (1989) 419–428.
[40] Q.L. Feng, F.P. Glasser, Microstructure, mass transport and densification of slag cement pastes, Mat Res Soc Symp Proc 178 (1990) 57–65.
[41] I.G. Richardson, The nature of the hydration products in hardened cements, in: Proc. Joe Cabrera Symp. on Durability of Materials, 6th CANMET/ACI Int. Conf. on Fly Ash, Silica Fume, Slag, and Natural Pozzolans in Concrete, Ed. R.N. Swamy, Bangkok, Thailand, May 31–June 5, (1998) 13–37.
[42] K.L. Scrivener, H.H. Patel, P.L. Pratt, L.J. Parrott, Analysis of phases in cement paste using backscattered electron images, methanol adsorption and thermogravimetric analysis, Mat Res Soc Symp Proc 85 (1985) 67–76.
[43] H. Zhao, D. Darwin, Quantitative backscattered electron analysis of cement paste, Cem Concr Res 22 (1992) 695–706.
[44] D. Bonen, A discussion of the paper "Quantitative backscattered electron analysis of cement paste," by H. Zhao and D. Darwin, Cem Concr Res 23 (1993) 749–757.
[45] G.W. Groves, Transmission electron microscopy of cements and mortars, Materials Forum, 14 (1990) 1–8.
[46] G.W. Groves, S.A. Rodger, The hydration of C_3S and ordinary Portland cement with relatively large additions of microsilica, Adv Cem Res 2(8) (1989) 135–140.
[47] A.M. Harrisson, N.B. Winter, H.F.W. Taylor, An examination of some pure and composite Portland cement pastes using scanning electron microscopy with X-ray analytical capability, Proc. 8th Int. Cong. Chem. Cem., IV (1986) 170–175.
[48] D. Bonen, S. Diamond, Interpretation of compositional patterns found by quantitative energy dispersive X-ray analysis for cement paste constituents, J Am Ceram Soc 77(7) (1994) 1875–1882.
[49] D.L. Rayment, A.J. Majumdar, The composition of the C-S-H phases in Portland cement pastes, Cem Conc Res 12 (1982) 753–764.
[50] I.G. Richardson, G.W. Groves, The incorporation of minor and trace elements into calcium silicate hydrate (C-S-H) gel in hardened cement pastes, Cem Concr Res 23 (1993) 131–138.
[51] H.F.W. Taylor, Proposed structure for calcium silicate hydrate gel, J Am Ceram Soc 69 (1986) 464–467.
[52] I.G. Richardson, G.W. Groves, Models for the composition and structure of calcium silicate hydrate (C-S-H) gel in hardened tricalcium silicate pastes, Cem Concr Res 22 (1992) 1001–1010.
[53] S.A. Rodger, G.W. Groves, N.J. Clayden, C.M. Dobson, A study of tricalcium silicate hydration from very early to very late stages, Mat Res Soc Symp Proc 85 (1987) 13–20.
[54] J.F. Young, Investigations of calcium silicate hydrate structure using ^{29}Si nuclear magnetic resonance spectroscopy. J Am Ceram Soc 71 (1988) C-118–C-120.
[55] L.S. Dent-Glasser, E.E. Lachowski, K. Mohan, H.F.W. Taylor, A multi-method study of C_3S hydration, Cem Concr Res 8 (1978) 733–740.
[56] L.S. Dent-Glasser, E.E. Lachowski, M.Y. Qureshi, H.P. Calhoun, D.J. Embree, W.D. Jamieson, C.R. Masson, Identification of some of the polysilicate components of trimethylsilylated cement paste, Cem Concr Res 11 (1981) 775–780.
[57] K. Mohan, H.F.W. Taylor, A trimethylsilylation study of tricalcium silicate pastes, Cem Concr Res 12 (1982) 25–31.
[58] J. Hirljac, Z.-Q. Wu, J.F. Young, Silicate polymerization during the hydration of alite, Cem Concr Res 13 (1983) 877–886.
[59] N.J. Clayden, C.M. Dobson, G.W. Groves, S.A. Rodger, The application of solid-state nuclear magnetic resonance spectroscopy techniques to the study of the hydration of tricalcium silicate, Proc. 8th Int Cong Chem Cem III (1986) 51–56.
[60] S.A. Rodger, G.W. Groves, N.J. Clayden, C.M. Dobson, Hydration of tricalcium silicate followed by ^{29}Si NMR with cross-polarization, J Am Ceram Soc 71(2) (1988) 91–96.
[61] E. Lippmaa, M. Mägi, M. Tarmak, W. Wieker, A.R. Grimmer, A high resolution ^{29}Si NMR study of the hydration of tricalcium silicate, Cem Concr Res 12 (1982) 597–602.
[62] E. Lippmaa, M. Magi, A. Samoson, G. Engelhardt, A.R. Grimmer, Structural studies of silicates by solid-state high resolution ^{29}Si NMR, J Am Chem Soc 102(15) (1980) 4889–4893.
[63] G. Engelhardt, D. Michel, High Resolution Solid-state NMR of Silicates and Zeolites, Wiley, New York, 1987.
[64] H. Uchikawa, S. Uchida, S. Hanehara, Effect of character of glass phase in blending components on their reactivity in calcium hydroxide mixture, Proc 8th Int Cong Chem Cem IV (1986) 245–250.
[65] S. Komarneni, R. Roy, D.M. Roy, C.A. Fyfe, G.J. Kennedy, A.A. Bothner-By, J. Dadok, A.S. Chesnick, ^{27}Al and ^{29}Si magic angle spin-

ning nuclear magnetic resonance spectroscopy of Al-substituted tobermorites, J Mat Sci 20 (1985) 4209–4214.
[66] M. Tsuji, S. Komarneni, P. Malla, Substituted tobermorites: ^{27}Al and ^{29}Si NMR, cation exchange, and water sorption studies, J Am Ceram Soc 74 (1991) 274–279.
[67] I.G. Richardson, A.R. Brough, R. Brydson, G.W. Groves, C.M. Dobson, The location of aluminum in substituted calcium silicate hydrate (C-S-H) gels as determined by ^{29}Si and ^{27}Al NMR and EELS, J Am Ceram Soc 76 (1993) 2285–2288.
[68] P.J. Schilling, L.G. Butler, A. Roy, H.C. Eaton, ^{29}Si and ^{27}Al MAS NMR of NaOH-activated blast-furnace slag, J Am Ceram Soc 77(9) (1994) 2363–2368.
[69] P. Faucon, T. Charpentier, A. Nonat, J.C. Petit, Triple-quantum two-dimensional ^{27}Al magic angle nuclear magnetic resonance study of the aluminium incorporation in calcium silicate hydrates, J Am Chem Soc 120 (1998) 12075–12082.
[70] P. Faucon, T. Charpentier, D. Bertrandie, A. Nonat, J. Virlet, J.C. Petit, Characterization of calcium aluminate hydrates and related hydrates of cement pastes by ^{27}Al MQ-MAS NMR, Inorg Chem 37 (1998) 3726–3733.
[71] P. Faucon, J.C. Petit, T. Charpentier, J.F. Jacquinot, F. Adenot, Silicon substitution for aluminum in calcium silicate hydrates, J Am Ceram Soc 82(5) (1999) 1307–1312.
[72] A.M. Dunster, J.R. Parsonage, M.J.K. Thomas, The pozzolanic reaction of metakaolinite and its effect on Portland cement hydration, J Mat Sci 28 (1993) 1345–1350.
[73] G.W. Groves, Microcrystalline calcium hydroxide in Portland cement pastes of low water/cement ratio, Cem Concr Res 11 (1981) 713–718.
[74] G.W. Groves, I.G. Richardson, Microcrystalline calcium hydroxide in pozzolanic cement pastes, Cem Concr Res 24 (1994) 1191–1196.
[75] R. Brydson, I.G. Richardson, D.W. McComb, G.W. Groves, Parallel electron energy loss spectroscopy study of Al-substituted calcium silicate hydrate (C-S-H) phases present in hardened cement pastes, Solid State Communications, 88 (1993) 183–187.
[76] G. Mascolo, O. Marino, MgO-bearing phases in the hydration products of slag cement. Proc. 7th Int Cong Chem Cem II (1980) III–58–III62.
[77] G.W. Brindley, S.M. Kikkawa, A crystal-chemical study of Mg, Al and Ni, Al hydroxy-perchlorates and hydroxy-carbonates. Am Mineral 64 (1979) 836–843.
[78] H.F.W. Taylor, Nanostructure of C-S-H: Current status, Adv Cem Bas Mater 1 (1993) 38–46.